ACS EARTH AND SPACE CHEMISTRY

http://pubs.acs.org/journal/aesccq

Article

Quantum Chemical and Kinetic Study of the Gas-Phase Reactions of Methane Sulfonamide with Cl Atom and the Fate of $^{\bullet}CH_2S(=O)_2NH_2$ with $^3O_2$ in the Atmosphere

Parandaman Arathala and Rabi A. Musah*

Cite This: *ACS Earth Space Chem.* 2023, 7, 1049−1059

Read Online

ACCESS | Metrics & More | Article Recommendations | Supporting Information

ABSTRACT: The gas phase mechanism of the chlorine atom ($^{\bullet}Cl$)-initiated oxidation of methane sulfonamide ($CH_3S(=O)_2NH_2$; MSAM) has been elucidated using ab initio/DFT electronic structure methods and chemical kinetic modeling. A reaction that commences via abstraction of an H-atom from the methyl group of MSAM to form a transition state with a barrier height of ∼4.8 kcal mol^{-1} above that of the MSAM + $^{\bullet}Cl$ reactants, yielding $^{\bullet}CH_2S(=O)_2NH_2$ + HCl was found to be a major path in comparison with the other possibilities. Rate coefficients for all possible H-atom abstraction reactions were calculated using the canonical variational transition state theory (CVT) with the small curvature tunneling (SCT) method in the temperature range of 200−400 K. The rate coefficient for the major reaction was found to be 1.6×10^{-14} cm^3 molecule^{-1} s^{-1} at 300 K, while the overall rate coefficient for the MSAM + $^{\bullet}Cl$ reaction is found to be 1.7×10^{-14} cm^3 molecule^{-1} s^{-1} at 300 K. In addition, SCT contributions, branching ratios for each reaction path, and the atmospheric implications are provided and discussed. Based on the results, the MSAM + $^{\bullet}Cl$ reaction proceeds to form $^{\bullet}CH_2S(=O)_2NH_2$, which then further reacts with $^3O_2$ under oxygen-rich conditions to form the corresponding RO_2 adduct ($^{\bullet}OOCH_2S(=O)_2NH_2$). Subsequent reactions of this radical result in the formation of greenhouse gases such as sulfur dioxide (SO_2), carbon dioxide (CO_2), carbon monoxide (CO), nitric acid (HNO_3), nitrous oxide (N_2O), and formic acid (HC(O)OH), which may contribute to climate change and formation of secondary organic aerosols and acid rain.

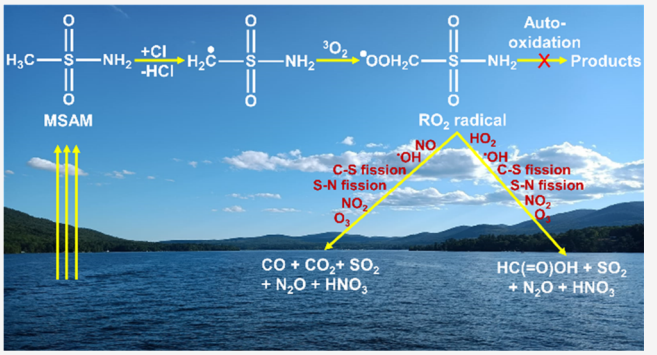

KEYWORDS: *methane sulfonamide, chlorine atom, rate coefficient, canonical variational transition state theory, small curvature tunneling, atmospheric lifetime, sulfur dioxide*

1. INTRODUCTION

Chlorine atoms ($^{\bullet}Cl$) are the most reactive oxidants in the atmosphere. They are involved in the transformation of volatile organic compounds (VOCs)[1−3] and affect the tropospheric ozone (O_3) budget.[4−6] They are also involved in facilitating secondary organic aerosol (SOA) formation.[7] Therefore $^{\bullet}Cl$ influences the earth's climate and air quality. Heterogeneous reactions involving sea salt generate Cl atoms.[8−10] Nitryl chloride ($ClNO_2$), a $^{\bullet}Cl$ source, is formed when dinitrogen pentoxide (N_2O_5) reacts with chloride-containing aerosols.[11] This is then followed by photolysis to generate $^{\bullet}Cl$ and NO_2 in the atmosphere. Another reported source of Cl atoms is the photolysis of molecular chlorine (Cl_2) derived from the reaction of ozone (O_3) with wet sea salt aerosols.[12] Further, significant amounts of Cl_2 (∼150 ppt) and HOCl have been observed in the marine boundary layer (MBL) and in the Arctic Sea,[13,14] and their photolysis is anticipated to generate Cl atoms in the MBL. In addition, hydrochloric acid (HCl), methyl chloride (CH_3Cl), carbonyl chloride ($COCl_2$), chloroform ($CHCl_3$), chlorocarbons, hydrochloroflurocarbons (HCFCs), and several other chlorine-containing molecules act as Cl atom sources in urban atmospheres.[10] Several studies indicate the $^{\bullet}Cl$ reactions are more important in facilitating understanding of the fate of VOCs in the atmosphere. The rate coefficients for the reactions of VOCs with the $^{\bullet}Cl$ atom are approximately an order of magnitude larger (with some exceptions) compared to the corresponding hydroxyl radical ($^{\bullet}OH$).[15−18] However, the concentration of $^{\bullet}Cl$ is ∼1 to 10% that of $^{\bullet}OH$ in the MBL.[19,20] Nevertheless, $^{\bullet}Cl$ reactions can be very important in understanding the removal of atmospheric pollutants in the MBL, as well as in polluted midcontinental regions and industrial locations.[21−23]

Received: January 5, 2023
Revised: March 16, 2023
Accepted: March 17, 2023
Published: April 4, 2023

There are several ubiquitous sulfur and nitrogen compounds that are emitted from the oceans. Examples include dimethyl sulfide (CH_3SCH_3—DMS), dimethyl sulfoxide ($CH_3S(=O)CH_3$—DMSO), alkyl amines (R-NH_2), nitrous oxide (N_2O), and ammonia (NH_3).[24−30] This suggests that the existence of such sulfur and nitrogen compounds in coastal regions may significantly impact global sulfur and nitrogen cycles.[31−34] An example is methane sulfonamide ($CH_3S(=O)_2NH_2$—MSAM), an S- and N-containing trace molecule that was detected recently over the Arabian sea with a maximum concentration of ∼60 parts per trillion (ppt).[35] It was suggested that the major source of this compound is ocean microbe-mediated reactions with DMS.[35]

To the best of our knowledge, there is no report on the atmospheric oxidation of MSAM with the Cl atom. However, OH radical reactions of MSAM have appeared. A recent experimental study described $^{\bullet}$OH-initiated photooxidation of MSAM carried out in a photochemical reactor at 298 K and 700 Torr total pressure,[36] and MSAM and its oxidation products were detected in situ by Fourier transform infrared (FTIR) spectroscopy. The reaction rate coefficient was reported to be $k = (1.4 \pm 0.3) \times 10^{-13}$ cm^3 molecule^{-1} s^{-1} using the relative rate technique at 298 K.[36] The MSAM + $^{\bullet}$OH reaction was proposed to proceed via methyl group H-atom abstraction as the dominant initial step.[36] Oxidation of MSAM with $^{\bullet}$OH under atmospheric conditions has also been studied using computational calculations.[37] All site-specific H-atom abstraction channel rate coefficients were calculated using canonical variational transition state theory and small curvature tunneling (CVT/SCT) approximation. The MSAM + $^{\bullet}$OH reaction rate coefficient was computed to be 1.2×10^{-13} cm^3 molecule^{-1} s^{-1} at 300 K.[37] The reaction mechanism proposed, which was based on the energetics and kinetic results, proceeds by abstraction of an H-atom from the $-NH_2$ group of MSAM yielding an N-centered MSAM radical + H_2O as major products.[37]

Even though the concentration of $^{\bullet}$OH is more than one order of magnitude larger compared to the concentration of Cl atom in the atmosphere, the overall atmospheric degradation of MSAM in the urban and coastal areas is anticipated to be facilitated to a significant extent by its reactions with $^{\bullet}$Cl, since the rate coefficient of the latter reaction is expected to be approximately one order of magnitude larger than the corresponding reaction with $^{\bullet}$OH. Given the importance of energetics and kinetic parameters in facilitating the understanding of the atmospheric chemistry of MSAM with respect to its reactions with Cl atoms, we studied this reaction mechanism using high-level quantum chemistry calculations. Accordingly, in the present work, all possible reaction channels and the overall reaction rate coefficients, in addition to the branching ratios for the $^{\bullet}$Cl reaction with MSAM between 200 and 400 K, were estimated. The results were then used to develop the most plausible mechanism for Cl atom-initiated oxidation of MSAM in the atmosphere.

2. COMPUTATIONAL METHODS

Geometry optimizations of reactants, prereactive complexes (PRCs), transition states (TSs), product complexes (INTs), and products involved in the H-atom abstraction and Cl addition paths were performed at the M06-2X/aug-cc-pV(T + d)Z level.[38,39] This hybrid density functional has been used in various studies to investigate reaction mechanisms, barrier heights, hydrogen bonding interactions, and kinetic parameters for various reactions of atmospheric interest.[18,40,41] We used the M06-2X/aug-cc-pV(T + d)Z level for computing harmonic vibrational frequencies for all of the stationary points. The obtained frequencies were then used to determine the local minima or transition states on the PESs. All transition states obtained in this work contain one negative frequency with all the others containing positive frequencies. Intrinsic reaction coordinate (IRC)[42] calculations were performed to make sure that the link between all the TSs and their corresponding PRCs and PCs on the minimum energy path was maintained. The CCSD(T)/aug-cc-pV(T + d)Z level was used to calculate more accurate single-point energies for all the stationary points.[43] The obtained CCSD(T)/aug-cc-pV(T + d)Z//M06-2X/aug-cc-pV(T + d)Z (CCSD(T)//M06-2X)-level energy values of all the minima and TSs were calculated relative to the energy of the separated starting reactants. The expectation that this approach would provide reasonably good energetic and rate parameters was based on results from our recent study of the reaction of $CH_3S(O)_2NH_2$ + $^{\bullet}$OH using the same level of theory, in which it was demonstrated that the obtained energies and rate coefficients agreed well with experimentally measured values.[37] Our recent work and other literature reports indicate that the CCSD(T)//M06-2X level with the same basis set (aug-cc-pV(T + d)Z) typically provides energies that are accurate to within 1 kcal mol^{-1}.[37,44] All the electronic structure calculations (ab initio/density functional theory) were carried out with the Gaussian 16 package.[45]

3. RESULTS AND DISCUSSION

The most stable structure of MSAM that was reported at the M06-2X/aug-cc-pV(T + d)Z level was used to perform the present calculations (see Figure 1).[37] Conformational analysis revealed that the preferred orientation of the H-atoms of the $-NH_2$ moiety is to be aligned toward the O-atoms of the SO_2 group through hydrogen bonding interactions (i.e., the *cis* orientation).

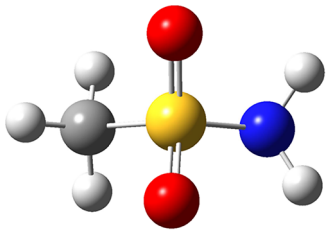

Figure 1. Most stable structure for methane sulfonamide optimized at the M06-2X/aug-cc-pV(T + d)Z level. The black, yellow, white, blue, and red colors represent C, S, H, N, and O-atoms, respectively (see geometry of *cis*-MSAM in Table S1).

In principle, atmospheric $^{\bullet}$Cl can react with MSAM via H-abstraction and/or Cl addition paths as illustrated in eqs 1−3. Eq 1 illustrates $^{\bullet}$Cl abstraction of an H-atom from the methyl moiety of MSAM to form $^{\bullet}CH_2S(O)_2NH_2$ + hydrochloric acid (HCl). The other H-atom abstraction provided in eq 2 features $^{\bullet}$Cl abstraction of an H-atom from the $-NH_2$ moiety of MSAM, to form an N-centered MSAM radical ($CH_3S(O)_2N^{\bullet}H$) + HCl. Eq 3 shows the formation of a methyl radical ($^{\bullet}CH_3$) and $ClS(O)_2NH_2$ as products as a consequence of $^{\bullet}$Cl addition to the S-atom of MSAM, followed by S−C single-bond fission.

https://doi.org/10.1021/acsearthspacechem.3c00004
ACS Earth Space Chem. 2023, 7, 1049−1059

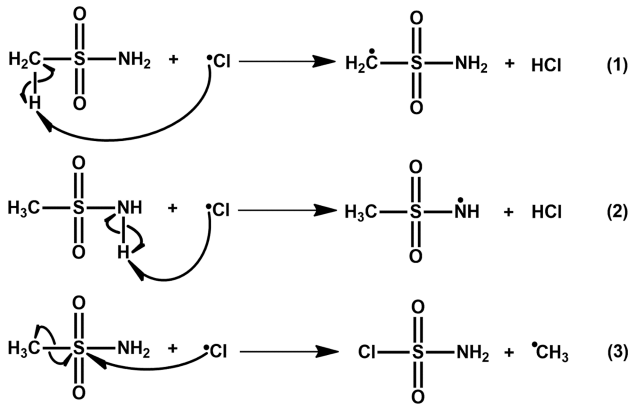

3.1. Initial Reactions of MSAM with Cl Atoms. The zero-point energy (ZPE) corrected PES profile for the two possible H-atom abstraction paths and the corresponding structures of the PRCs, TSs, INTs, and products involved in the MSAM and •Cl reaction are depicted in Figure 2. The

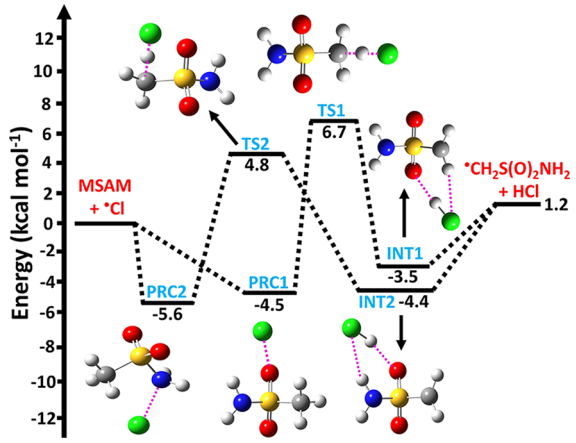

Figure 2. Zero-point corrected potential energy curves for the abstraction of an H-atom from the methyl group of methane sulfonamide by Cl atom leading to the formation of $^{\bullet}CH_2S(=O)_2NH_2$ + HCl. The energies on the potential were calculated at the CCSD(T)/aug-cc-pV(T + d)Z//M06-2X/aug-cc-pV(T + d)Z level. PRC1 and PRC2 refer to prereactive complexes; TS1 and TS2 refer to transition states; and INT1 and INT2 refer to product complexes. The black, yellow, white, green, blue, and red colors in the structures represent C, S, H, Cl, N, and O-atoms, respectively.

energies of all the stationary points were estimated relative to the energy of MSAM and •Cl as starting reactants at the CCSD(T)//M06-2X level. The corresponding energies are displayed in Figure 2. The total electronic energies (E_{total}) and corresponding ZPEs computed at the CCSD(T) and M06-2X levels are summarized in Table S2. All of the transition state imaginary frequencies, rotational constants, vibrational frequencies, and the optimized geometries of all of the stationary points obtained at the M06-2X level are displayed in Tables S1−S5. The potential energy profile for the two possible H-abstraction paths is shown in Figure 2. This PES featured in the figure indicates that the MSAM and Cl atom reactants initially undergo association to produce PRC1 and PRC2 with energies of −4.5 and −5.6 kcal mol^{-1} relative to the starting reactants, which are shown at the entrance channels in each PES. The greater stability of PRC1 and PRC2 is mainly due to the weak interactions between: (a) the Cl atom and the oxygen atom of MSAM, with a Cl−O bond distance of ∼2.58 Å; and (b) the Cl atom and N-atom of MSAM, with a bond distance of ∼2.43 Å (see PRC1 and PRC2 structures in Figure 2). In PRC1 and PRC2, these weak interactions, which are illustrated with a dotted line in the structures, are due to 2-center-3-electron (2c−3e) bond formation between the nitrogen or oxygen atom lone pair electrons and the single electron occupied p-orbital of the •Cl atom. Similar complexes have been reported in the literature for dimethyl sulfoxide, monoethanolamine, methylamine, dimethylamine, and trimethylamine with Cl atom reactions.[20,46,47] The Cl−N bond length in PRC2 is ∼0.2 Å shorter than the Cl−O bond in PRC1. This leads to greater stability of PRC2 by ∼1.1 kcal mol^{-1} compared to the value for PRC1. The two H-abstraction paths further lead to product complexes (INT1 and INT2) through the corresponding TS1 and TS2, with reaction barriers of 6.7 and 4.8 kcal mol^{-1}, respectively. The INTs then dissociate to $^{\bullet}CH_2S(=O)_2NH_2$ + HCl products. The transition state barriers (see Figure 2) indicate that H-abstraction from the $-CH_3$ group of MSAM via TS2 is the major reaction path for the formation of $^{\bullet}CH_2S(=O)_2NH_2$ + HCl products, since it is ∼2 kcal mol^{-1} lower in energy than the path that proceeds through TS1.

H-atom abstraction from the $-NH_2$ group of MSAM is also possible for the MSAM + Cl atom reaction. Figure 3 shows the

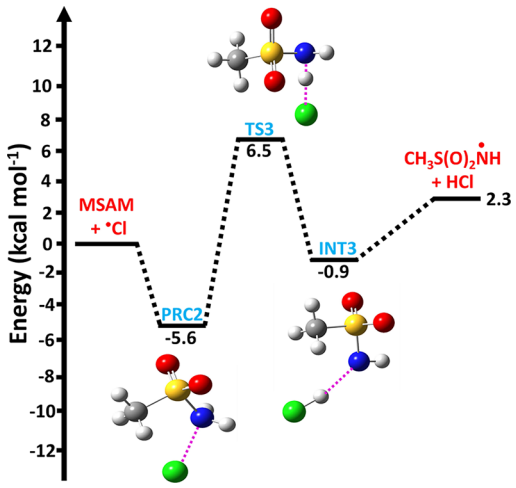

Figure 3. Zero-point corrected potential energy curve for the abstraction of an H-atom from the amine group of methane sulfonamide by Cl atom, leading to the formation of an N-centered methane sulfonamide radical + HCl products. The energies on the potential were calculated at the CCSD(T)/aug-cc-pV(T + d)Z//M06-2X/aug-cc-pV(T + d)Z level. The symbols PRC2, TS3, and INT3 refers to prereactive complex, transition state, and product complex, respectively. The black, yellow, white, green, blue, and red colors on the structures represent C, S, H, Cl, N, and O-atoms, respectively.

PES profile for this reaction calculated at the zero-point corrected CCSD(T)//M06-2X level. This reaction path initially proceeds through the MSAM and Cl atom reactants to produce a barrierless PRC2 with a binding energy of ∼ −5.6 kcal mol^{-1} relative to the energy of the initial reactants. This then leads to the formation of a TS3 with a barrier height of ∼6.5 kcal mol^{-1} above the MSAM + Cl atom reactants. TS3 further advances to form a product complex (INT3) which leads to the products $CH_3S(=O)_2N^{\bullet}-H$ and HCl. The energy barriers of all of the H-abstraction transition states

https://doi.org/10.1021/acsearthspacechem.3c00004
ACS Earth Space Chem. 2023, 7, 1049−1059

studied in the MSAM + Cl atom reaction suggest that abstraction of a methyl group H-atom by Cl atom through TS2 to form $^{\bullet}CH_2S(=O)_2NH_2$ + HCl is the major path when compared to all others that are possible.

Previous studies indicate that dimethyl sulfide, dimethyl sulfone, dimethyl thiosulfinate, and dipropyl thiosulfinate undergo addition reactions with Cl atoms.[18,48−50] Therefore, we also performed calculations for the addition channel represented by eq 3. Accordingly, the PRC, TS, INT, and products associated with the MSAM + $^{\bullet}$Cl addition channel were characterized. The obtained ZPE-corrected potential energy profile containing key stationary points for this reaction is shown in Figure 4. The M06-2X/aug-cc-pV(T + d)Z-level

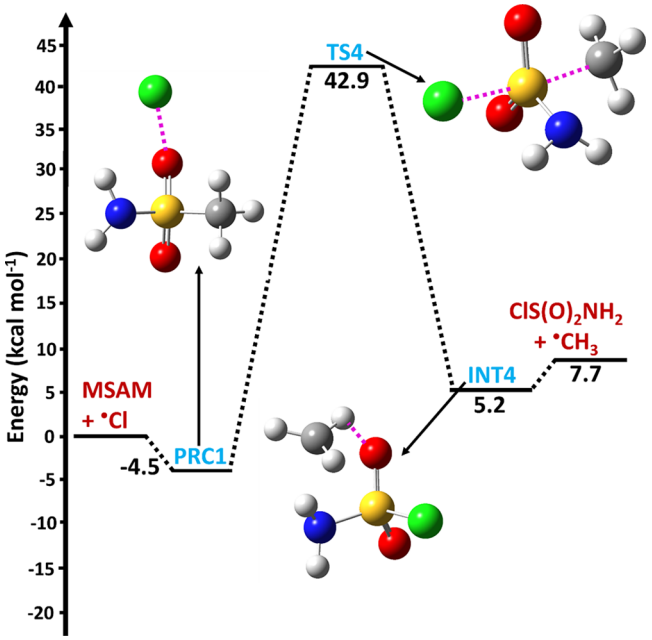

Figure 4. Zero-point corrected potential energy curve for the addition of Cl-atom to the S-atom of MSAM, leading to the formation of $^{\bullet}CH_3$ + $ClS(O)_2NH_2$ as products. The energies of all the stationary points on the potential were calculated at the CCSD(T)/aug-cc-pV(T + d)Z//M06-2X/aug-cc-pV(T + d)Z level. The symbols PRC1, TS4, and INT4 refer to prereactive complex, transition state, and product complex, respectively. The black, yellow, white, green, blue, and red colors represent C, S, H, Cl, N, and O-atoms, respectively.

optimized structures are presented in the figure. The results suggest that the addition reaction commences with the formation of PRC1 and then proceeds to a transition state (TS4) with a barrier height of ∼43.0 kcal mol^{-1}. This then leads to the formation of a product complex (INT4), to ultimately produce products $^{\bullet}CH_3$ + $ClS(O)_2NH_2$ at 7.7 kcal mol^{-1} above the starting reactants (MSAM and Cl atom). PRC1, TS4, and INT4 in the figure clearly indicate the propensity of the Cl atom to attack the S-atom of MSAM, resulting in S—C single-bond cleavage to form $^{\bullet}CH_3$ + $ClS(O)_2NH_2$ as products. However, the high barrier height on this potential would make this path inaccessible under atmospheric conditions, and as such, this reaction was not further considered in the performed calculations.

The product complexes (INT1 and INT2) that are formed between TS1 and $^{\bullet}CH_2S(O)_2NH_2$ + HCl, and TS2 and $^{\bullet}CH_2S(O)_2NH_2$ + HCl, have corresponding energies of 3.5 and 4.4 kcal mol^{-1}, respectively, below the energy of the starting MSAM + $^{\bullet}$Cl reactants (see Figure 2). INT1 is stabilized by two hydrogen bonds (O···H−Cl and −CH···Cl−H) with bond lengths of 1.92 and 2.85 Å, respectively. For INT2, the computed bond distances for the hydrogen bonding interactions (O···H−Cl and −NH···Cl−H) were 1.90 and 2.56 Å, respectively. The stability of INT2 is ∼1 kcal mol^{-1} higher than the value of INT1 (see Figure 2). This is mainly due to the presence of strong hydrogen bond interactions in INT2. A product complex (INT3) was identified between TS3 and $CH_3S(O)_2N^{\bullet}H$ + HCl products which was 0.9 kcal mol^{-1} below the starting MSAM + $^{\bullet}$Cl reactants (see Figure 3). It is stabilized by a −HN···HCl hydrogen bond interaction with a distance predicted to be 2.09 Å. A product complex between TS4 and $ClS(O)_2NH_2$ + $^{\bullet}CH_3$ (i.e., INT4) was identified at 5.2 kcal mol^{-1} above the energy of starting reactants (see Figure 4). It is stabilized by a −O···HCH_2 interaction with a bond length predicted to be ∼2.71 Å.

4. KINETICS

Two abstraction channels in the oxidation of MSAM by Cl atom, namely, abstraction of an H-atom from the methyl group to produce $^{\bullet}CH_2S(O)_2NH_2$ + HCl (eq 1) and the abstraction from an H-atom of the amine group leading to $CH_3S(O)_2N^{\bullet}H$ + HCl (eq 2), were described previously. In order to get a better understanding of the atmospheric fate of MSAM with respect to Cl atoms, as well as acquire information about the various products formed following its oxidation, the rate coefficients for these two H-abstraction pathways were determined. Their PES profiles (illustrated in Figures 2 and 3) suggested that they occur via two major steps: (i) the MSAM and Cl atom reactants weakly bind to form the respective PRC, which is in equilibrium with the initial reactants and (ii) the PRC proceeds to form a product complex (INT) through a transition state (TS) with a well-defined barrier. These two reaction steps are presented in eq 4.

$$\text{MSAM} + {}^{\bullet}\text{Cl} \underset{k_{-1}}{\overset{k_1}{\rightleftharpoons}} \text{PRC} \xrightarrow{k_2} \text{INT} \qquad (4)$$

In eq 4, k_1 and k_{-1} are the forward and reverse rate coefficients for the formation of PRC from the reaction of MSAM + Cl atom, respectively, which is in equilibrium with the reactants (MSAM + $^{\bullet}$Cl); k_2 is the unimolecular rate coefficient for the formation of INT from PRC via a transition state. The product of the unimolecular rate coefficients (k_2 in s^{-1}) and equilibrium constants (K_{eq} in cm^3 molecule^{-1}) provides bimolecular rate coefficients (k in cm^3 molecule^{-1} s^{-1}) in the atmospherically relevant temperatures using eq 5. This equation was derived by considering that the PRC is in equilibrium with the reactants (MSAM and Cl atom), and that it exists under steady-state conditions. Previous studies have utilized a similar approach for calculating the rate coefficients in the presence of bimolecular reactants.[51−54]

$$k = \left(\frac{k_1}{k_{-1}}\right)k_2 = K_{eq}k_2 \qquad (5)$$

The symbol K_{eq} in eq 5 is the equilibrium constant for the combination of the two reactants that leads to the formation of PRC that is shown in the first step of eq 4, and it can be defined using $K_{eq} = \frac{k_1}{k_{-1}}$. The rate coefficient ($k_2$) is calculated using CVT[55−57] combined with the small curvature tunneling[58] (SCT) method through eq 6. These calculations were performed with Polyrate (2016)[59] kinetic code.

https://doi.org/10.1021/acsearthspacechem.3c00004
ACS Earth Space Chem. 2023, 7, 1049−1059

$$k_{uni}^{CVT/SCT} = \Gamma \frac{k_B T}{h} \frac{Q_{TS}(s^*)}{Q_{PRC}} \exp^{-V(s^*)/RT} \quad (6)$$

The temperature-dependent equilibrium constant (K_{eq}) for the formation of PRCs from the initial reactants was calculated using eq 7

$$K_{eq} = \frac{Q_{PRC}}{Q_{MSAM} Q_{Cl}} \exp^{-(E_{PRC} - E_{MSAM} - E_{Cl})/RT} \quad (7)$$

The Q symbols in eqs 6 and 7 are the product of individual partition functions of the MSAM, Cl atom, PRCs, and TSs. Standard statistical mechanics formulas were used to calculate the partition functions.[60] Other symbols in eqs 6 and 7 are as follows: E (represents the ZPE-corrected CCSD(T)//M06-2X energies); R and T correspond to the gas constant and temperature (K) respectively; Γ refers to the SCT transmission coefficient; k_B is the Boltzmann constant; and h is Plank's constant. The potential energy at the barrier maximum is represented by $V(s^*)$, and the value of the reaction path at the free energy maximum is denoted by s^*.

4.1. Rate Coefficients for the Reaction of MSAM + Cl Atom. The MSAM + Cl atom reaction channel rate coefficients were calculated using the vibrational frequencies obtained by the M06-2X/aug-cc-pV(T + d)Z level, and zero-point corrected CCSD(T)//M06-2X energies for all the species present on the PESs. The calculated temperature-dependent unimolecular rate coefficients (k_2) and equilibrium constants (K_{eq}) for the formation of possible PRCs from the MSAM + Cl atom reaction are displayed in Tables S6 and S7. The rate coefficients (in cm^3 $molecule^{-1}$ s^{-1}) for the two H-abstraction channels associated with the oxidation of MSAM with Cl atom reactions in the temperature range of 200 and 400 K are displayed in Table 1. The structure of MSAM indicates that not all the H-atoms attached to the methyl group are equivalent. This is a consequence of the presence of the oxygen atoms in the SO_2 group and the orientation of the hydrogen atoms in the methyl group with respect to these oxygens. Thus, hydrogen abstraction from the methyl group by the Cl atom may proceed by different paths. By considering the oxygen atoms of the SO_2 group as the frame of reference, two possible transition state configurations were found (i.e., TS1 and TS2 (see Figure 2)). The structure of TS1 indicates that the hydrogen atom that is abstracted by the Cl atom is oriented *toward* the oxygen atoms of the SO_2 group, whereas for TS2, the abstracted hydrogen is positioned *away* from the O-atoms of the SO_2 (see the structures of TS1 and TS2 in Figure 2). The transition state geometries and energies of TS1 and TS2 are significantly different. This clearly indicates that TS1 and TS2 represent two different hydrogen abstraction transition states for the methyl group hydrogen abstraction paths. The results for the energy barriers indicate that TS1 is ~2 kcal mol^{-1} higher than the value of TS2. The lack of consideration of this difference in energy barriers would clearly lead to significant errors in the computed rate coefficients. If just one of them is considered, and the reaction path degeneracy is assumed to be 3, then a large disagreement would arise between the computed rate coefficients and the experimentally observed ones. Stated differently, the calculated value would be significantly underestimated if only TS1 is considered, and significantly overestimated if only TS2 is considered. Therefore, both were considered, and the reaction path degeneracy was 2 for the TS2 pathway and 1 for the TS1 pathway. On the other hand, the orientation with respect to the SO_2 oxygens of the two hydrogen atoms attached to the N-atom of $-NH_2$ group is such that they are equivalent, and the yield transition state structure TS3 is shown in Figure 3. These two hydrogens are equivalent, and hence, the reaction path degeneracy becomes 2 for the TS3 pathway. For this reason, the contribution of the rate coefficients via k_{TS2} and k_{TS3} was multiplied by 2 (see Table 1).

Table 1. Calculated Bimolecular Rate Coefficients (in cm^3 $molecule^{-1}$ s^{-1}) for the Three Possible H-Atom Abstraction Paths and the Overall Rate Coefficients[a] for the MSAM + Cl Atom Reaction in the Temperatures between 200 and 400 K

T (K)	k_{TS1}	k_{TS2}[b]	k_{TS3}[b]	$k_{total}^{MSAM + Cl}$
200	6.78×10^{-19}	6.56×10^{-16}	1.97×10^{-18}	6.58×10^{-16}
210	1.33×10^{-18}	1.00×10^{-15}	4.00×10^{-18}	1.01×10^{-15}
220	2.50×10^{-18}	1.48×10^{-15}	7.65×10^{-18}	1.49×10^{-15}
230	4.47×10^{-18}	2.14×10^{-15}	1.40×10^{-17}	2.16×10^{-15}
240	7.71×10^{-18}	3.02×10^{-15}	2.44×10^{-17}	3.05×10^{-15}
250	1.28×10^{-17}	4.16×10^{-15}	4.11×10^{-17}	4.22×10^{-15}
260	2.06×10^{-17}	5.64×10^{-15}	6.63×10^{-17}	5.73×10^{-15}
270	3.21×10^{-17}	7.52×10^{-15}	1.04×10^{-16}	7.65×10^{-15}
280	4.88×10^{-17}	9.82×10^{-15}	1.60×10^{-16}	1.00×10^{-14}
290	7.25×10^{-17}	1.27×10^{-14}	2.37×10^{-16}	1.31×10^{-14}
298	9.86×10^{-17}	1.56×10^{-14}	3.23×10^{-16}	1.60×10^{-14}
300	1.05×10^{-16}	1.63×10^{-14}	3.45×10^{-16}	1.67×10^{-14}
400	1.87×10^{-15}	1.13×10^{-13}	5.94×10^{-15}	1.21×10^{-13}

[a]The overall rate coefficients ($k_{total}^{MSAM + Cl}$) for the MSAM + •Cl reaction is obtained by adding the rate coefficients for all the individual reaction paths at the corresponding temperatures. [b]The contribution of the rate coefficients via k_{TS2} and k_{TS3} was multiplied by 2.

The results in Table 1 indicate a trend of increasing rate coefficients with increasing temperature for both abstraction paths. This is mainly due to the positive transition state barriers, which varied between ~4.8 and 6.7 kcal mol^{-1} relative to the reactants for all H-abstraction channels. The bimolecular rate coefficients for product ($^{\bullet}CH_2S(O)_2NH_2$ + HCl) formation from the MSAM + Cl atom reaction that proceeds through TS2, is ~2 to 3 orders of magnitude larger than it is for the other possible paths in the presently studied temperature range. For example, calculated reaction rate coefficients for the H-abstraction channels that proceed via TS1, TS2, and TS3 at 200 K were found to be 6.8×10^{-19}, 6.6×10^{-16}, and 2.0×10^{-18} cm^3 $molecule^{-1}$ s^{-1}, respectively. On the other hand, the bimolecular rate coefficients for the same reaction paths at 300 K were found to be 1.1×10^{-16}, 1.6×10^{-14}, and 3.5×10^{-16} cm^3 $molecule^{-1}$ s^{-1}, respectively. In addition, overall rate coefficients of the MSAM + Cl atom reaction were calculated by adding the present studied H-atom abstraction path rate coefficients at each temperature in the present studied temperature range. Thus, the calculated overall rate coefficients in the temperature range of 200−400 K are displayed in Table 1 and plotted in Figure 5. The CCSD(T)//M06-2X levels typically provide energies that are accurate to within 1 kcal mol^{-1}. We believe that the error in the present calculated rate coefficients is ~2 times in the temperatures between 200 and 300 K. However, this uncertainty in the rate coefficients does not influence the conclusions drawn in this work. The results from Table 1 and Figure 5 indicate a positive temperature dependence of the rate coefficients in the studied temperature range. For example, the overall rate coefficients for

https://doi.org/10.1021/acsearthspacechem.3c00004
ACS Earth Space Chem. 2023, 7, 1049−1059

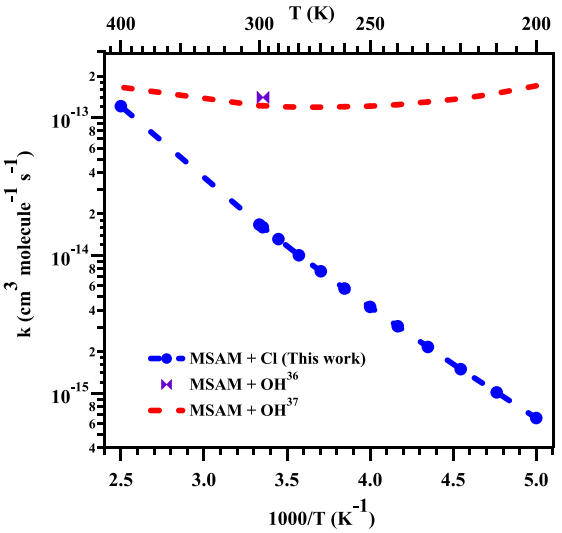

Figure 5. Overall rate coefficients calculated for the MSAM + Cl atom reaction compared with the overall rate coefficient values for the MSAM + OH radical reaction in the temperature range of 200−400 K.[37] The experimentally reported MSAM + OH radical reaction rate coefficient[36] at 298 K is also included for comparison.

the MSAM + Cl atom reaction at 200 and 300 K were found to be 6.6×10^{-16} and 1.7×10^{-14} cm^3 molecule^{-1} s^{-1}, respectively. This is mainly due to the positive transition state barriers for all the H-atom abstraction paths. Experimentally measured MSAM + Cl atom reaction rate coefficients were not available for comparison with the present calculated values. Therefore, the MSAM + Cl atom reaction rate coefficients computed in this work were compared with values of theoretically calculated rate coefficients for the MSAM oxidation initiated by $^{\bullet}$OH[37] in the studied range of temperatures, and the value of the experimentally measured rate coefficient for the reaction of MSAM with OH radical at 298 K.[36] The results clearly suggest that the overall rate coefficients for the MSAM + Cl atom reaction are smaller than the values for the theoretically calculated MSAM + OH radical reaction in the same temperature range[37] and also smaller than the experimentally measured MSAM reactions with OH radical at 298 K temperatures.[36] For example, in the present work, the overall rate coefficient at 298 K for the MSAM + $^{\bullet}$Cl reaction was found to be 1.6×10^{-14} cm^3 molecule^{-1} s^{-1}, which is ∼8 times smaller than that for the theoretically calculated and experimentally measured MSAM + OH radical reaction at the same temperature.[36,37] The MSAM oxidation in the presence of $^{\bullet}$OH that is reported in the literature[37] and the MSAM + Cl atom reaction studied in this work used similar methods and the same level of theory to calculate the rate coefficients. The smaller rate coefficients for the reaction of MSAM + $^{\bullet}$Cl are mainly due to the following two factors: (1) the presence in each of the MSAM + OH radical abstraction paths of a hydrogen-bonded PRC that is ∼1 kcal mol^{-1} more stable when compared to the values for PRCs formed for the analogous reaction involving MSAM + $^{\bullet}$Cl, and (2) the transition state for the MSAM oxidation initiated by OH radical reaction being stabilized by strong hydrogen bonding interactions, with reaction barriers that were found to be ∼2 to 4 kcal mol^{-1} lower than the values computed in this work for the transition states involved in the MSAM + Cl atom reaction.[37] The absence of hydrogen bonding interactions leads to the high reaction barrier transition states that were identified for the MSAM + Cl reaction. The present results indicate that $^{\bullet}$Cl is less reactive than the OH radical for the transformation of MSAM under atmospheric conditions. However, several studies indicate that $^{\bullet}$Cl has higher reactivity toward the removal of VOCs although its concentration is lower than that of the OH radical.[9,23,61−63]

The rate coefficients reported in the literature for various volatile organosulfur compounds (VOSCs) with respect to their reactions with Cl atoms at 298 K were compared with the value of the present MSAM + Cl atom reaction at the same temperature. The present MSAM + Cl atom reaction rate coefficient was found to be ∼3 to 4 orders of magnitude lower compared to the values for the DMS (CH_3SCH_3) + Cl atom reaction (reported to be $k = (3.6 \pm 0.2) \times 10^{-10}$ cm^3 molecule^{-1} s^{-1}),[64] and the DMSO ($CH_3S(O)CH_3$) + Cl atom reaction (reported to be $k = (7.4 \pm 1.0) \times 10^{-11}$ cm^3 molecule^{-1} s^{-1})[65] at 298 K. At the same time, the rate coefficient for the present reaction is close to the value for the dimethyl sulfone ($CH_3S(O)_2CH_3$; $DMS(O)_2$) + Cl atom reaction, which is reported to be $k = (2.4 \pm 0.8) \times 10^{-14}$ cm^3 molecule^{-1} s^{-1} at the same temperature.[65]

In addition, the SCT factor was estimated for each abstraction path and its contribution to their respective reaction rate coefficients is provided in Table S8. The results presented in the table reveal that the tunneling factor decreases with increasing temperature from 200 to 400 K. For example, the SCT contributions to each site-specific reaction via TS1, TS2, and TS3 were found to be 17.5, 27.1, and 11.1 at 200 K and 4.1, 5.4, and 3.4 at 300 K, respectively.

To further understand the mechanism of the MSAM + Cl atom reaction, the temperature dependence of the branching ratios for each reaction path was calculated in the 200−400 K temperature range. This was done based on the ratios of the rate coefficient for each site-specific reaction to the total rate coefficient at the same temperature. The obtained branching ratios for each H-atom abstraction path in the temperature range of 200−400 K are provided in Table S9. The results show that the branching ratio for the reaction that proceeds via TS2 makes the highest contribution to the overall reaction when compared to the other possible channels (i.e., ∼99.6% at 200 K, which decreases to ∼97.3% at 300 K). The contribution to the overall reaction from the other possible H-atom abstraction paths via TS1 and TS3 increases with increasing temperature. For example, the contributions of TS1 and TS3 to the overall reaction are 0.1 and 0.3% at 200 K and 0.6 and 2.1% at 300 K, respectively. Overall, the results indicate that the reaction resulting in the C-centered MSAM radical + HCl products is major when compared to all of the other possible paths at the atmospherically relevant temperatures.

The lifetime of MSAM with Cl atom was derived using the equation: $\tau = 1/(k[\mathrm{Cl}])$.[66] In this equation, k is the rate coefficient for the MSAM + $^{\bullet}$Cl reaction, and the tropospheric concentration of $^{\bullet}$Cl used in this calculation was $[\mathrm{Cl}] = 1.3 \times 10^5$ radical cm^{-3}.[13] This value was chosen because the concentration of Cl atoms in the marine boundary layer has been found to be 1−10% of the concentration of $^{\bullet}$OH.[19,20,23] The overall rate coefficients calculated here were used to determine the lifetime of MSAM with Cl atom in the present studied temperature range. The atmospheric lifetime of MSAM in its reactions with $^{\bullet}$Cl atom was estimated to be ∼2 to 370 years in the temperatures between 200 and 400 K. A recent study reported that MSAM is not photolyzed at a measurable rate by the 254 nm radiation.[36] It was concluded that the

https://doi.org/10.1021/acsearthspacechem.3c00004
ACS Earth Space Chem. 2023, 7, 1049−1059

tropospheric photolysis of MSAM as a removal process is not a significant sink, since actinic flux only at wavelengths above 320 nm is available in the troposphere.[36] Therefore, the removal of MSAM under tropospheric conditions mainly depends on its reactions with OH radicals and Cl atoms.

In addition, we also calculated the atmospheric lifetime of MSAM with respect to OH and Cl atoms at 298 K using eq 8.[67]

$$\frac{1}{\tau_{\text{eff}}} = \frac{1}{\tau_{\text{OH}}} + \frac{1}{\tau_{\text{Cl}}} \quad (8)$$

where τ_{eff} is the cumulative atmospheric lifetime of MSAM, and τ_{OH} and τ_{Cl} are the lifetimes of MSAM due to its reactions with OH radical and Cl atoms, respectively. We used the experimentally measured MSAM + OH radical reaction rate coefficient[36] that was reported to be 1.4×10^{-13} cm^3 molecule^{-1} s^{-1}, the present MSAM + $^{\bullet}$Cl reaction rate coefficient calculated to be 1.6×10^{-14} cm^3 molecule^{-1} s^{-1} at 298 K, and the average atmospheric concentrations of [OH] and [Cl] of 1×10^6 and 1.3×10^5 radical cm^{-3}, respectively.[13,68] The lifetime of MSAM with the OH radical using these data was estimated to be 83 days, and the cumulative atmospheric lifetime of MSAM with respect to its reactions with OH radicals and Cl atoms was estimated to be ~81 days at 298 K. This suggests that OH radical reactions are primarily responsible for the atmospheric loss of MSAM when compared to its reactions with Cl atoms.

4.2. $^{\bullet}CH_2S(=O)_2NH_2 + {}^3O_2$ Reaction. The energetics and rate coefficient data in the present work indicate that the abstraction of an H-atom from the methyl group of MSAM by $^{\bullet}$Cl to form $^{\bullet}CH_2S(O)_2NH_2$ + HCl is dominant under atmospheric conditions. Branching ratios revealed that this path contributes up to 97% of the total transformation of MSAM with Cl atom at 300 K. Therefore, to gain a more complete understanding of the fate of $^{\bullet}CH_2S(=O)_2NH_2$, we further explored its possible subsequent reactions under atmospheric conditions.

The formed $^{\bullet}CH_2S(=O)_2NH_2$ is a carbon-centered radical product. Based on the literature, the dominant fate of C-centered radical products in the atmosphere is mostly due to their reaction with ground-state oxygen ($^3O_2$) molecules,[36,69,70] a consequence of the large concentration of oxygen that is present in the atmosphere. Once released, $^{\bullet}CH_2S(=O)_2NH_2$ can rapidly react with O_2 to form the RO_2 (R = $CH_2S(=O)_2NH_2$) radical adduct. Thus, the atmospheric chemistry of $^{\bullet}CH_2S(=O)_2NH_2$ in the presence of O_2 was investigated using the same CCSD(T)//M06-2X-level calculations described earlier. The spin contamination $\langle S^2 \rangle$ and T1 diagnostic values for all the species involved in the $^{\bullet}CH_2S(=O)_2NH_2 + {}^3O_2$ reaction are given in Table S10 of the Supporting Information. The results indicate that the $\langle S^2 \rangle$ values for the open-shell systems are in the range of 0.753–0.762 before annihilation, while those after annihilation turn out to be 0.75. The $\langle S^2 \rangle$ value for triplet species was found to be 2.01, which is also smaller than the allowed value (≤2.05).[71] This suggests that there is almost no contribution from spin contamination. In addition, T1 diagnostic values for all the species involved in the $^{\bullet}CH_2S(=O)_2NH_2 + {}^3O_2$ reaction indicate that these values are smaller than the allowed value of 0.044, except for TS6 (0.046) (see Table S10).[72] These results strongly indicate that the multireference character in the CCSD(T) wave functions is negligible. The ZPE-corrected potential energy profile for the $^{\bullet}CH_2S(=O)_2NH_2 + {}^3O_2$ reaction is depicted in Figure 6. All of the TSs, intermediates,

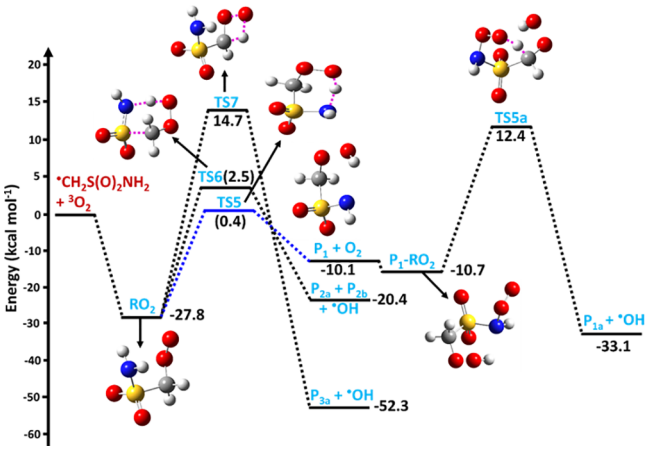

Figure 6. Zero-point corrected potential energy curves for the $^{\bullet}CH_2S(=O)_2NH_2 + {}^3O_2$ reaction leading to the formation of various products, computed at the CCSD(T)/aug-cc-pV(T + d)Z//M06-2X/aug-cc-pV(T + d)Z level. The black, yellow, white, blue, and red colors represent C, S, H, N, and O-atoms, respectively.

and products involved in the $^{\bullet}CH_2S(=O)_2NH_2$ and O_2 reaction are illustrated in Figure 6. All of the minima and the TSs in the figure were optimized at the M06-2X level with the aug-cc-pV(T + d)Z basis set. The zero-point corrected CCSD(T)//M06-2X-level computed energies of all the stationary points on the PES are displayed in the figure, and all the values were estimated with respect to the $^{\bullet}CH_2S(=O)_2NH_2 + O_2$ separated reactants. Figure 6 indicates that the most stable RO_2 radical adduct is formed through attack by atmospheric O_2 on the C-site of $^{\bullet}CH_2S(=O)_2NH_2$ via a barrierless reaction with a binding energy of ~ −27.8 kcal mol^{-1} with respect to the energy of the $^{\bullet}CH_2S(=O)_2NH_2 + {}^3O_2$ reactants (see Figure 6). We compared the binding energy of this RO_2 radical adduct with that of the RO_2 radical formed from the C-centered radical of the $CH_3S(=O)C^{\bullet}H_2 + O_2$ reaction. We found the $OOCH_2S(=O)_2NH_2$ radical to be less stable than the $CH_3S(=O)CH_2OO$ radical by ~1.8 kcal mol^{-1}. The binding energy for the formation of the latter was reported to be ~ −29.6 kcal mol^{-1} at the CBS-QB3 level relative to the energy of $CH_3S(=O)C^{\bullet}H_2 + O_2$ reactants.[73]

The formed RO_2 radical adduct can react further by two possible transformation pathways: (i) H-atom transfer reactions and (ii) reactions with hydroperoxyl (HO_2) radical or nitric oxide (NO). These are discussed below:

4.2.1. H-Atom Transfer Reactions. By virtue of the H-atoms that are present within the $-CH_2$ and $-NH_2$ moieties of the RO_2 radical, a number of intramolecular hydrogen transfer reactions are possible. These are illustrated in eqs 9–11.

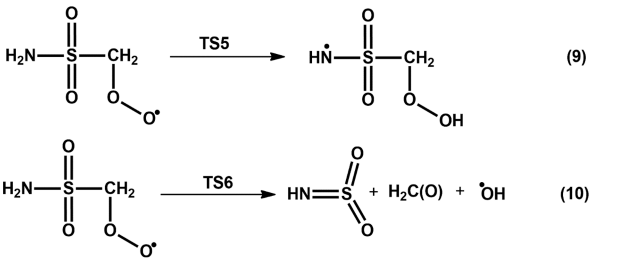

https://doi.org/10.1021/acsearthspacechem.3c00004
ACS Earth Space Chem. 2023, 7, 1049–1059

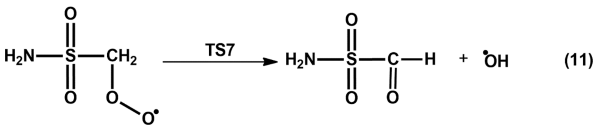

Migration of a hydrogen atom from $-NH_2$ to the terminal oxygen of the RO_2 adduct through TS5 with a 0.4 kcal mol^{-1} barrier relative to the $^{\bullet}CH_2S(=O)_2NH_2$ + O_2 reactants is shown in eq 9 and Figure 6. TS5 then leads to the formation of the N-centered QOOH radical (Q = $^{\bullet}NHS(O)_2CH_2-$), which is located at −10.1 kcal mol^{-1} on the PES. The QOOH radical formed in the previous step further reacts with O_2 to form a new peroxy radical ($HOOQO_2$). Various studies indicate that H-atom transfer within the RO_2 radical, followed by O_2 addition, leads to the production of highly oxygenated organic compounds (HOMs).[74,75] The formed $HOOQO_2$ then further undergoes migration of H-atom to the terminal O-atom of $HOOQO_2$ through a transition state (TS5a) with a barrier height of 12.4 kcal mol^{-1}. The reaction then finally forms $HC(O)S(O)_2NHOOH$ (P1a) + OH radical at −33.1 kcal mol^{-1}. A second option involves autooxidation of RO_2 through H-atom transfer from the $-NH_2$ group to the terminal O-atom, followed by cleavage of the S−C and O−O single bonds in a concerted manner through TS6, with a barrier height of ∼2.5 kcal mol^{-1} (calculated at the same level of theory—see eq 10 and Figure 6). This then leads to the formation of $HNS(O)_2$ (P_{2a}) + $H_2C(O)$ (P_{2b}) + $^{\bullet}OH$ as final products. In a third possible pathway, the RO_2 radical adduct undergoes autooxidation through an H-atom shift from the $-CH_2$ group to the terminal oxygen atom of RO_2, followed by the dissociation of the O−O single bond (see eq 11 and Figure 6) through TS7, with a barrier height of 14.7 kcal mol^{-1} above that of the $^{\bullet}CH_2S(=O)_2NH_2$ + O_2 reactants. This leads to the formation of OH radical + P_{3a} ($H_2NS(O)_2C(O)H$) products, located at −52.3 kcal mol^{-1} on the PES profile (Figure 6). The results shown on the PES in Figure 6 suggest that the reaction in which $^{\bullet}CH_2S(=O)_2NH_2$ + $^3O_2$ leads to the RO_2 adduct, and which is followed by H-atom transfer via TS5 to form the QOOH radical (P_1), is the one that is most energetically favored, compared to the other possible H-atom transfer reactions. To verify this conclusion, we calculated the first-order rate coefficients for the unimolecular reactions given in eqs 9−11 at 298 K and 1 atm pressure using the Mesmer kinetic code.[76] This kinetic code uses the master equation method for calculating the time-, temperature-, and pressure-dependent rate coefficients for multienergy well reaction systems. We used RRKM theory for calculating the rate coefficients for all tight transition states associated with the $^{\bullet}CH_2S(=O)_2NH_2$ + $^3O_2$ reaction. The input parameters used in the calculations are vibrational frequencies and rotational constants for all the stationary points involved in the $^{\bullet}CH_2S(=O)_2NH_2$ + $^3O_2$ reaction, computed at the M06-2X/aug-cc-pV(T + d)Z and ZPE corrected CCSD(T)//M06-2X levels (see Tables S4 and S5 and Figure 6). As mentioned previously, the error in the reaction barriers is within 1 kcal mol^{-1}, and the uncertainty in the calculated rate coefficients is ∼2 times. The obtained rate coefficients were found to be 1.5 × 10^{-7}, 2.3 × 10^{-9}, and 5.0 × 10^{-11} s^{-1}, respectively. These results indicate that QOOH radical formation from the RO_2 radical adduct is ∼2 to 4 orders of magnitude faster compared to the other studied H-atom transfer channels associated with RO_2 radical adduct.

4.2.2. Reaction of the RO_2 Radical Adduct with HO_2 Radical and NO. In addition to the aforementioned hydrogen transfer reactions, bimolecular reactions of the RO_2 radical with HO_2 and NO could also be important, to the extent that they compete with the autooxidation of RO_2 radicals under atmospheric conditions. Both reactions (i.e., RO_2 + HO_2 and RO_2 + NO to form the corresponding hydroperoxide (ROOH; R = $H_2NS(O)_2CH_2$-) + O_2 and alkoxy radical ($RO^{\bullet}$; R = $H_2NS(O)_2CH_2$-) + nitrogen dioxide (NO_2) products, respectively) are shown in eqs 12 and 13.

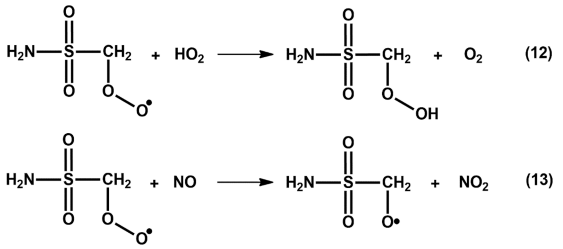

The rate coefficients for the typical RO_2 + HO_2 and RO_2 + NO reactions at 298 K are reported to be 8.1 × 10^{-12} and 9.0 × 10^{-12} cm^3 $molecule^{-1}$ s^{-1}, respectively.[77,78] The concentration of HO_2 and NO in urban areas, the remote pristine atmosphere, and in indoor air are reported to be 40 and 100 ppt, respectively.[79−81] Thus, we calculated the pseudo-first-order rate coefficients for the typical RO_2 + HO_2 and RO_2 + NO reactions at 298 K by using the reported RO_2 + HO_2 and RO_2 + NO reaction rate coefficients and the HO_2 and NO concentrations in urban areas, remote pristine atmosphere, and indoor air. The obtained pseudo-first-order rate coefficients at 298 K for the $H_2NS(O)_2CH_2OO^{\bullet}$ + HO_2 radical and $H_2NS(O)_2CH_2OO^{\bullet}$ + NO reactions were found to be ∼8.14 × 10^{-3} and 2.30 × 10^{-2} s^{-1}, respectively. These results indicate that the $H_2NS(O)_2CH_2OO^{\bullet}$ + HO_2 radical reaction is ∼10^4−10^8 times, and the $H_2NS(O)_2CH_2OO^{\bullet}$ + NO reaction is 10^5−10^9 times faster than the intramolecular H-atom transfer reactions.

4.3. Reaction Mechanism of MSAM + Cl Atom. Based on the results of the calculations described above, we propose the most plausible reaction mechanism for the MSAM + Cl atom reaction. Initially, MSAM undergoes oxidation initiated by the Cl atom to form the $^{\bullet}CH_2S(O)_2NH_2$ along with HCl. Once formed, $^{\bullet}CH_2S(O)_2NH_2$ reacts with O_2 under oxygen-rich conditions to form the $^{\bullet}OOCH_2S(O)_2NH_2$ adduct. Based on the present results, intramolecular H-atom transfer reactions of this adduct are slow, and thus, the fate of the $^{\bullet}OOCH_2S(O)_2NH_2$ adduct depends on the concentrations of HO_2 and NO in the atmosphere. The HO_2 and NO concentrations in indoor air, urban, and the remote pristine atmosphere are reported to be ∼40 and less than 100 ppt, respectively.[79−81] Therefore, the $^{\bullet}OOCH_2S(O)_2NH_2$ adduct reacts with HO_2 and NO to produce the corresponding hydroperoxide ($HOOCH_2S(O)_2NH_2$) + O_2, and alkoxy radical ($H_2NS(O)_2CH_2O^{\bullet}$) + NO_2, respectively. The fate of $HOOCH_2S(O)_2NH_2$ has been reported in the literature.[36] The findings suggest that atmospheric $^{\bullet}OH$ abstracts an H-atom from $-CH_2$, leading to the formation of $HOOC^{\bullet}HS(O)_2NH_2$ + H_2O products. The formed $HOOC^{\bullet}HS(O)_2NH_2$ proceeds via C−S bond scission to generate formic acid (HC(O)OH) and SO_2NH_2.[36] The fate of the alkoxy radical ($H_2NS(O)_2CH_2O^{\bullet}$) has also been reported,[36] and suggests that atmospheric O_2 abstracts a hydrogen from the $-CH_2$ group leading to the formation of $HC(O)S(O)_2NH_2$ + HO_2. The

https://doi.org/10.1021/acsearthspacechem.3c00004
ACS Earth Space Chem. 2023, 7, 1049−1059

$HC(O)S(O)_2NH_2$ further reacts with OH radical, which is followed by C−S bond cleavage leading to the formation of $S(O)_2NH_2$ + carbon monoxide (CO). In an alternative path, $H_2NS(O)_2CH_2O^\bullet$ undergoes S−C bond cleavage to form SO_2NH_2 + CH_2O.[36] The formed CH_2O reacts with $^\bullet$OH and O_2 in tandem to produce CO, which then reacts with $^\bullet$OH to form carbon dioxide (CO_2) as the final product. It has also been reported that the formed common product SO_2NH_2 further proceeds to S−N bond cleavage to generate sulfur dioxide (SO_2) + NH_2 radical.[36] The NH_2 radical then interacts with NO_2 to form nitrous oxide (N_2O) + H_2O. However, a second viable path for the NH_2 radical is to react with ozone (O_3), followed by reactions with OH, O_2, and HO_2 radicals, leading to the formation of nitric acid (HNO_3) as the final product.[36] The results of the present work indicate that MSAM in the presence of Cl atom leads to the formation of the greenhouse gases SO_2, formic acid, nitric acid, CO, CO_2, and N_2O as final products. As such, MSAM and its final products may contribute to climate change, acid rain, and secondary organic aerosol (SOA) formation.

5. CONCLUSIONS

The atmospheric oxidation of MSAM initiated by Cl atoms was investigated using high-level computational methods and chemical kinetic modeling. Our results indicate that the MSAM + $^\bullet$Cl reaction that proceeds via H-atom abstraction from the $-CH_3$ moiety of MSAM by the Cl atom to form $^\bullet CH_2S(=O)_2NH_2$ + HCl is energetically more dominant. The rate coefficients for the hydrogen abstraction channels in the title reaction were calculated using the CVT/SCT method in the temperature range of 200−400 K. The overall rate coefficient for the MSAM + Cl atom reaction was calculated to be 1.6×10^{-14} cm^3 $molecule^{-1}$ s^{-1} at 298 K. While the atmospheric lifetime of MSAM with respect to its reaction of Cl atom was found to be 2−370 years in the temperature range of 200−400 K, the cumulative atmospheric lifetime of MSAM with respect to OH radicals and Cl atoms was calculated to be 81 days at 298 K. The results of investigations of subsequent transformations of $^\bullet CH_2S(=O)_2NH_2$ in the presence of O_2, HO_2, and NO revealed the formation of SO_2, HC(O)OH, HNO_3, N_2O, CO, and CO_2 as the greenhouse gas end products. Thus, MSAM released from the oceans may have major effects on climate change, the formation of acid rain, and SOAs in the atmosphere.

■ ASSOCIATED CONTENT

Supporting Information

The Supporting Information is available free of charge at https://pubs.acs.org/doi/10.1021/acsearthspacechem.3c00004.

Optimized geometries of all the stationary points, total electronic energies including zero-point energy corrections calculated at various levels of theory, imaginary frequencies of various TSs at the M06-2X level, rotational constants at the M06-2X level, vibrational frequencies, unimolecular rate coefficients, equilibrium constants, tunneling contributions, branching ratios for all possible paths, and spin contamination and T1 diagnostic values (PDF)

■ AUTHOR INFORMATION

Corresponding Author

Rabi A. Musah − *Department of Chemistry, University at Albany—State University of New York, Albany, New York 12222, United States;* orcid.org/0000-0002-3135-4130; Email: rmusah@albany.edu

Author

Parandaman Arathala − *Department of Chemistry, University at Albany—State University of New York, Albany, New York 12222, United States;* orcid.org/0000-0002-9818-9686

Complete contact information is available at: https://pubs.acs.org/10.1021/acsearthspacechem.3c00004

Notes

The authors declare no competing financial interest.

■ ACKNOWLEDGMENTS

The financial support of the National Science Foundation (grant numbers 1310350 and 1710221) to R.A.M. is gratefully acknowledged. The authors thank the High-Performance Computing Center at the University at Albany-SUNY for their support, as well as the Research Foundation for SUNY.

■ REFERENCES

(1) Aschmann, S. M.; Atkinson, R. Rate constants for the gas-phase reactions of alkanes with Cl atoms at 296 ± 2 K. *Int. J. Chem. Kinet.* **1995**, *27*, 613−622.

(2) Nelson, L.; Rattigan, O.; Neavyn, R.; Sidebottom, H.; Treacy, J.; Nielsen, O. J. Absolute and relative rate constants for the reactions of hydroxyl radicals and chlorine atoms with a series of aliphatic alcohols and ethers at 298 K. *Int. J. Chem. Kinet.* **1990**, *22*, 1111−1126.

(3) Wang, L.; Arey, J.; Atkinson, R. Reactions of chlorine atoms with a series of aromatic hydrocarbons. *Environ. Sci. Technol.* **2005**, *39*, 5302−5310.

(4) Chang, S.; Allen, D. T. Atmospheric chlorine chemistry in southeast Texas: Impacts on ozone formation and control. *Environ. Sci. Technol.* **2006**, *40*, 251−262.

(5) Knipping, E. M.; Dabdub, D. Impact of chlorine emissions from sea-salt aerosol on coastal urban ozone. *Environ. Sci. Technol.* **2003**, *37*, 275−284.

(6) Tanaka, P. L.; Riemer, D. D.; Chang, S.; Yarwood, G.; McDonald-Buller, E. C.; Apel, E. C.; Orlando, J. J.; Silva, P. J.; Jimenez, J. L.; Canagaratna, M. R.; Neece, J. D.; Mullins, C. B.; Allen, D. T. Direct evidence for chlorine-enhanced urban ozone formation in Houston, Texas. *Atmos. Environ.* **2003**, *37*, 1393−1400.

(7) Platt, U.; Hönninger, G. The role of halogen species in the troposphere. *Chemosphere* **2003**, *52*, 325−338.

(8) Finlayson-Pitts, B. J. Chlorine chronicles. *Nat. Chem.* **2013**, *5*, 724−724.

(9) Faxon, C. B.; Allen, D. T. Chlorine chemistry in urban atmospheres: A review. *Environ. Chem.* **2013**, *10*, 221−233.

(10) Keene, W. C.; Khalil, M. A. K.; Erickson, D. J., III; McCulloch, A.; Graedel, T. E.; Lobert, J. M.; Aucott, M. L.; Gong, S. L.; Harper, D. B.; Kleiman, G.; et al. Composite global emissions of reactive chlorine from anthropogenic and natural sources: Reactive chlorine emissions inventory. *J. Geophys. Res.* **1999**, *104*, 8429−8440.

(11) Finlayson-Pitts, B. J.; Ezell, M. J.; Pitts, J. N. Formation of chemically active chlorine compounds by reactions of atmospheric NaCl particles with gaseous N_2O_5 and $ClONO_2$. *Nature* **1989**, *337*, 241−244.

(12) Oum, K. W.; Lakin, M. J.; DeHaan, D. O.; Brauers, T.; Finlayson-Pitts, B. J. Formation of molecular chlorine from the photolysis of ozone and aqueous sea-salt particles. *Science* **1998**, *279*, 74−76.

(13) Spicer, C. W.; Chapman, E. G.; Finlayson-Pitts, B. J.; Plastridge, R. A.; Hubbe, J. M.; Fast, J. D.; Berkowitz, C. M. Unexpectedly high concentrations of molecular chlorine in coastal air. *Nature* **1998**, *394*, 353−356.
(14) Pszenny, A. A. P.; Keene, W. C.; Jacob, D. J.; Fan, S.; Maben, J. R.; Zetwo, M. P.; Springer-Young, M.; Galloway, J. N. Evidence of inorganic chlorine gases other than hydrogen chloride in marine surface air. *Geophys. Res. Lett.* **1993**, *20*, 699−702.
(15) Atkinson, R.; Baulch, D. L.; Cox, R. A.; Hampson, R. F., Jr.; Kerr (Chairman), J. A.; Troe, J. Evaluated kinetic and photochemical data for atmospheric chemistry: Supplement III. IUPAC subcommittee on gas kinetic data evaluation for atmospheric chemistry. *J. Phys. Chem. Ref. Data* **1989**, *18*, 881−1097.
(16) Wang, W.; Ezell, M. J.; Ezell, A. A.; Soskin, G.; Finlayson-Pitts, B. J. Rate constants for the reactions of chlorine atoms with a series of unsaturated aldehydes and ketones at 298 K: Structure and reactivity. *Phys. Chem. Chem. Phys.* **2002**, *4*, 1824−1831.
(17) Arathala, P.; Musah, R. A. Computational study investigating the atmospheric oxidation mechanism and kinetics of dipropyl thiosulfinate initiated by OH radicals and the fate of propanethiyl radical. *J. Phys. Chem. A* **2020**, *124*, 8292−8304.
(18) Arathala, P.; Musah, R. A. Oxidation of dipropyl thiosulfinate initiated by Cl radicals in the gas phase: Implications for atmospheric chemistry. *ACS Earth Space Chem.* **2021**, *5*, 2878−2890.
(19) Wingenter, O. W.; Sive, B. C.; Blake, N. J.; Blake, D. R.; Rowland, F. S. Atomic chlorine concentrations derived from ethane and hydroxyl measurements over the equatorial Pacific Ocean: Implication for dimethyl sulfide and bromine monoxide. *J. Geophys. Res.* **2005**, *110*, 1−10.
(20) Nicovich, J. M.; Mazumder, S.; Laine, P. L.; Wine, P. H.; Tang, Y.; Bunkan, A. J. C.; Nielsen, C. J. An experimental and theoretical study of the gas phase kinetics of atomic chlorine reactions with CH_3NH_2, $(CH_3)_2NH$, and $(CH_3)_3N$. *Phys. Chem. Chem. Phys.* **2015**, *17*, 911−917.
(21) Stutz, J.; Ezell, M. J.; Ezell, A. A.; Finlayson-Pitts, B. J. Rate constants and kinetic isotope effects in the reactions of atomic chlorine with n-butane and simple alkenes at room temperature. *J. Phys. Chem. A* **1998**, *102*, 8510−8519.
(22) Arathala, P.; Musah, R. A. Thermochemistry and kinetics of the atmospheric oxidation reactions of propanesulfinyl chloride initiated by OH radicals: A computational approach. *J. Phys. Chem. A* **2022**, *126*, 4264−4276.
(23) Xie, H.-B.; Ma, F.; Wang, Y.; He, N.; Yu, Q.; Chen, J. Quantum chemical study on •Cl-initiated atmospheric degradation of monoethanolamine. *Environ. Sci. Technol.* **2015**, *49*, 13246−13255.
(24) Voss, M.; Bange, H. W.; Dippner, J. W.; Middelburg, J. J.; Montoya, J. P.; Ward, B. The marine nitrogen cycle: Recent discoveries, uncertainties and the potential relevance of climate change. *Philos. Trans. R. Soc. B* **2013**, *368*, No. 20130121.
(25) Ge, X.; Wexler, A. S.; Clegg, S. L. Atmospheric amines − Part I. A review. *Atmos. Environ.* **2011**, *45*, 524−546.
(26) Gibb, S. W.; Mantoura, R. F. C.; Liss, P. S. Ocean-atmosphere exchange and atmospheric speciation of ammonia and methylamines in the region of the NW Arabian Sea. *Global Biogeochem. Cycles* **1999**, *13*, 161−178.
(27) Arévalo-Martínez, D. L.; Steinhoff, T.; Brandt, P.; Körtzinger, A.; Lamont, T.; Rehder, G.; Bange, H. W. N_2O emissions from the northern benguela upwelling system. *Geophys. Res. Lett.* **2019**, *46*, 3317−3326.
(28) Johnson, M. T.; Liss, P. S.; Bell, T. G.; Lesworth, T. J.; Baker, A. R.; Hind, A. J.; Jickells, T. D.; Biswas, K. F.; Woodward, E. M. S.; Gibb, S. W. Field observations of the ocean-atmosphere exchange of ammonia: Fundamental importance of temperature as revealed by a comparison of high and low latitudes. *Global Biogeochem. Cycles* **2008**, *22*, GB1019.
(29) Paulot, F.; Jacob, D. J.; Johnson, M. T.; Bell, T. G.; Baker, A. R.; Keene, W. C.; Lima, I. D.; Doney, S. C.; Stock, C. A. Global oceanic emission of ammonia: Constraints from seawater and atmospheric observations. *Global Biogeochem. Cycles* **2015**, *29*, 1165−1178.
(30) Carpenter, L. J.; Archer, S. D.; Beale, R. Ocean-atmosphere trace gas exchange. *Chem. Soc. Rev.* **2012**, *41*, 6473−6506.
(31) Brimblecombe, P. The Global Sulfur Cycle. In *Treatise on Geochemistry*, 2nd ed.; Elsevier: Amsterdam, 2014; pp. 559−591.
(32) Bentley, R.; Chasteen, T. G. Environmental VOSCs−−formation and degradation of dimethyl sulfide, methanethiol and related materials. *Chemosphere* **2004**, *55*, 291−317.
(33) Sievert, S. M.; Kiene, R. P.; Schulz-Vogt, H. N. The sulfur cycle. *Oceanography* **2007**, *20*, 117−123.
(34) Fowler, D.; Steadman, C. E.; Stevenson, D.; Coyle, M.; Rees, R. M.; Skiba, U. M.; Sutton, M. A.; Cape, J. N.; Dore, A. J.; Vieno, M.; et al. Effects of global change during the 21st century on the nitrogen cycle. *Atmos. Chem. Phys.* **2015**, *15*, 13849−13893.
(35) Edtbauer, A.; Stönner, C.; Pfannerstill, E. Y.; Berasategui, M.; Walter, D.; Crowley, J. N.; Lelieveld, J.; Williams, J. A new marine biogenic emission: Methane sulfonamide (MSAM), dimethyl sulfide (DMS), and dimethyl sulfone ($DMSO_2$) measured in air over the Arabian Sea. *Atmos. Chem. Phys.* **2020**, *20*, 6081−6094.
(36) Berasategui, M.; Amedro, D.; Edtbauer, A.; Williams, J.; Lelieveld, J.; Crowley, J. N. Kinetic and mechanistic study of the reaction between methane sulfonamide ($CH_3S(O)_2NH_2$) and OH. *Atmos. Chem. Phys.* **2020**, *20*, 2695−2707.
(37) Arathala, P.; Musah, R. A. Theoretical study of the atmospheric chemistry of methane sulfonamide initiated by OH radicals and the $CH_3S(O)_2N{\cdot}H + {}^3O_2$ reaction. *J. Phys. Chem. A* **2022**, *126*, 9447−9460.
(38) Zhao, Y.; Truhlar, D. G. The M06 suite of density functionals for main group thermochemistry, thermochemical kinetics, noncovalent interactions, excited states, and transition elements: Two new functionals and systematic testing of four M06-class functionals and 12 other functionals. *Theor. Chem. Acc.* **2008**, *120*, 215−241.
(39) Dunning, T. H., Jr.; Peterson, K. A.; Wilson, A. K. Gaussian basis sets for use in correlated molecular calculations. X. The atoms aluminum through argon revisited. *J. Chem. Phys.* **2001**, *114*, 9244−9253.
(40) Arathala, P.; Musah, R. A. Atmospheric oxidation of propanesulfinic acid initiated by OH radicals: Reaction mechanism, energetics, rate coefficients, and atmospheric implications. *ACS Earth Space Chem.* **2021**, *5*, 1498−1510.
(41) Chen, J.; Berndt, T.; Møller, K. H.; Lane, J. R.; Kjaergaard, H. G. Atmospheric fate of the CH_3SOO radical from the $CH_3S + O_2$ equilibrium. *J. Phys. Chem. A* **2021**, *125*, 8933−8941.
(42) Fukui, K. The path of chemical reactions - the IRC approach. *Acc. Chem. Res.* **1981**, *14*, 363−368.
(43) Noga, J.; Bartlett, R. J. The full CCSDT model for molecular electronic structure. *J. Chem. Phys.* **1987**, *86*, 7041−7050.
(44) Vereecken, L.; Francisco, J. S. Theoretical studies of atmospheric reaction mechanisms in the troposphere. *Chem. Soc. Rev.* **2012**, *41*, 6259−6293.
(45) Frisch, M. J.; Trucks, G. W.; Schlegel, H. B.; Scuseria, G. E.; Robb, M. A.; Cheeseman, J. R.; Scalmani, G.; Barone, V.; Petersson, G. A.; Nakatsuji, H.; et al. *Gaussian 16, Revision B.01*; Gaussian, Inc.: Wallingford, CT, 2016.
(46) Kleissas, K. M.; Nicovich, J. M.; Wine, P. H. Spectroscopy and kinetics of the gas phase addition complex of atomic chlorine with dimethyl sulfoxide. *J. Photochem. Photobiol., A* **2007**, *187*, 1−9.
(47) Nicovich, J. M.; Parthasarathy, S.; Pope, F. D.; Pegus, A. T.; McKee, M. L.; Wine, P. H. Kinetics, mechanism, and thermochemistry of the gas phase reaction of atomic chlorine with dimethyl sulfoxide. *J. Phys. Chem. A* **2006**, *110*, 6874−6885.
(48) Arathala, P.; Musah, R. A. Theoretical studies of the gas-phase reactions of S-methyl methanesulfinothioate (dimethyl thiosulfinate) with OH and Cl radicals: Reaction mechanisms, energetics, and kinetics. *J. Phys. Chem. A* **2019**, *123*, 8448−8459.
(49) Resende, S. M.; De Almeida, W. B. Theoretical study of the atmospheric reaction between dimethyl sulfide and chlorine atoms. *J. Phys. Chem. A* **1997**, *101*, 9738−9744.

(50) Vandresen, S.; Resende, S. M. The atmospheric reaction between DMSO and the chlorine radical. *J. Phys. Chem. A* **2004**, *108*, 2284−2289.
(51) Parandaman, A.; Tangtartharakul, C. B.; Kumar, M.; Francisco, J. S.; Sinha, A. A computational study investigating the energetics and kinetics of the HNCO + $(CH_3)_2NH$ reaction catalyzed by a single water molecule. *J. Phys. Chem. A* **2017**, *121*, 8465−8473.
(52) Arathala, P.; Musah, R. A. Catalytic effect of water and formic acid on the reaction of carbonyl sulfide with dimethyl amine under tropospheric conditions. *Phys. Chem. Chem. Phys.* **2021**, *23*, 8752−8766.
(53) Jørgensen, S.; Jensen, C.; Kjaergaard, H. G.; Anglada, J. M. The gas-phase reaction of methane sulfonic acid with the hydroxyl radical without and with water vapor. *Phys. Chem. Chem. Phys.* **2013**, *15*, 5140−5150.
(54) Galano, A.; Alvarez-Idaboy, J. R.; Bravo-Pérez, G.; Ruiz-Santoyo, M. E. Gas phase reactions of C_1−C_4 alcohols with the OH radical: A quantum mechanical approach. *Phys. Chem. Chem. Phys.* **2002**, *4*, 4648−4662.
(55) Garrett, B. C.; Truhlar, D. G. Variational transition state theory. Primary kinetic isotope effects for atom transfer reactions. *J. Am. Chem. Soc.* **1980**, *102*, 2559−2570.
(56) Garrett, B. C.; Truhlar, D. G. Criterion of minimum state density in the transition state theory of bimolecular reactions. *J. Chem. Phys.* **1979**, *70*, 1593−1598.
(57) Bao, J. L.; Truhlar, D. G. Variational transition state theory: Theoretical framework and recent developments. *Chem. Soc. Rev.* **2017**, *46*, 7548−7596.
(58) Liu, Y. P.; Lynch, G. C.; Truong, T. N.; Lu, D. H.; Truhlar, D. G.; Garrett, B. C. Molecular modeling of the kinetic isotope effect for the [1,5]-sigmatropic rearrangement of cis-1,3-pentadiene. *J. Am. Chem. Soc.* **1993**, *115*, 2408−2415.
(59) Zheng, J.; Bao, L.; Meana-Pañeda, R.; Zhang, S.; Lynch, G. C.; Corchado, J. C.; Chuang, Y. Y.; Fast, P. L.; Hu, W. P.; Liu, Y. P.; et al. *POLYRATE version 2016-2A*; University of Minnesota: Minneapolis, MN, 2016.
(60) McQuarrie, D. A. *Statistical Mechanics;* UniVersity Science Books: Sausalito, CA, 2000.
(61) Canosa-Mas, C. E.; Hutton-Squire, H. R.; King, M. D.; Stewart, D. J.; Thompson, K. C.; Wayne, R. P. Laboratory kinetic studies of the reactions of Cl atoms with species of biogenic origin: δ3-carene, isoprene, methacrolein and methyl vinyl ketone. *J. Atmos. Chem.* **1999**, *34*, 163−170.
(62) Finlayson-Pitts, B. J.; Keoshian, C. J.; Buehler, B.; Ezell, A. A. Kinetics of reaction of chlorine atoms with some biogenic organics. *Int. J. Chem. Kinet.* **1999**, *31*, 491−499.
(63) Ma, F.; Ding, Z.; Elm, J.; Xie, H.-B.; Yu, Q.; Liu, C.; Li, C.; Fu, Z.; Zhang, L.; Chen, J. Atmospheric oxidation of piperazine initiated by •Cl: Unexpected high nitrosamine yield. *Environ. Sci. Technol.* **2018**, *52*, 9801−9809.
(64) Enami, S.; Nakano, Y.; Hashimoto, S.; Kawasaki, M.; Aloisio, S.; Francisco, J. S. Reactions of Cl atoms with dimethyl sulfide: A theoretical calculation and an experimental study with cavity ring-down spectroscopy. *J. Phys. Chem. A* **2004**, *108*, 7785−7789.
(65) Falbe-Hansen, H.; Sørensen, S.; Jensen, N. R.; Pedersen, T.; Hjorth, J. Atmospheric gas-phase reactions of dimethylsulphoxide and dimethylsulphone with OH and NO_3 radicals, Cl atoms and ozone. *Atmos. Environ.* **2000**, *34*, 1543−1551.
(66) Kurylo, M. J.; Orkin, V. L. Determination of atmospheric lifetimes via the measurement of OH radical kinetics. *Chem. Rev.* **2003**, *103*, 5049−5076.
(67) Kumar, A.; Rajakumar, B. Cl Atom initiated photo-oxidation of mono-chlorinated propanes to form carbonyl compounds: A kinetic and mechanistic approach. *J. Phys. Chem. A* **2019**, *123*, 723−741.
(68) Atkinson, R. Atmospheric chemistry of VOCs and NOx. *Atmos. Environ.* **2000**, *34*, 2063−2101.
(69) Parandaman, A.; Kumar, M.; Francisco, J. S.; Sinha, A. Organic acid formation from the atmospheric oxidation of gem diols: Reaction mechanism, energetics, and rates. *J. Phys. Chem. A* **2018**, *122*, 6266−6276.
(70) Møller, K. H.; Berndt, T.; Kjaergaard, H. G. Atmospheric autoxidation of amines. *Environ. Sci. Technol.* **2020**, *54*, 11087−11099.
(71) Asatryan, R.; Bozzelli, J. W. Chain cranching and termination in the low-temperature combustion of n-alkanes: 2-pentyl radical + O_2, isomerization and association of the second O_2. *J. Phys. Chem. A* **2010**, *114*, 7693−7708.
(72) Lee, T. J.; Taylor, P. R. A diagnostic for determining the quality of single-reference electron correlation methods. *Int. J. Quant. Chem. Symp.* **1989**, *36*, 199−207.
(73) Asatryan, R.; Bozzelli, J. W. Formation of a Criegee intermediate in the low-temperature oxidation of dimethyl sulfoxide. *Phys. Chem. Chem. Phys.* **2008**, *10*, 1769−1780.
(74) Rissanen, M. P.; Kurtén, T.; Sipilä, M.; Thornton, J. A.; Kangasluoma, J.; Sarnela, N.; Junninen, H.; Jørgensen, S.; Schallhart, S.; Kajos, M. K.; et al. The formation of highly oxidized multifunctional products in the ozonolysis of cyclohexene. *J. Am. Chem. Soc.* **2014**, *136*, 15596−15606.
(75) Berndt, T.; Richters, S.; Jokinen, T.; Hyttinen, N.; Kurtén, T.; Otkjær, R. V.; Kjaergaard, H. G.; Stratmann, F.; Herrmann, H.; Sipilä, M.; et al. Hydroxyl radical-induced formation of highly oxidized organic compounds. *Nat. Commun.* **2016**, *7*, 13677.
(76) Glowacki, D. R.; Liang, C.-H.; Morley, C.; Pilling, M. J.; Robertson, S. H. MESMER: An open-source master equation solver for multi-energy well reactions. *J. Phys. Chem. A* **2012**, *116*, 9545−9560.
(77) Boyd, A. A.; Flaud, P.-M.; Daugey, N.; Lesclaux, R. Rate constants for RO_2 + HO_2 reactions measured under a large excess of HO_2. *J. Phys. Chem. A* **2003**, *107*, 818−821.
(78) Atkinson, R.; Arey, J. Atmospheric degradation of volatile organic compounds. *Chem. Rev.* **2003**, *103*, 4605−4638.
(79) Hofzumahaus, A.; Rohrer, F.; Lu, K.; Bohn, B.; Brauers, T.; Chang, C.-C.; Fuchs, H.; Holland, F.; Kita, K.; Kondo, Y.; et al. Amplified trace gas removal in the troposphere. *Science* **2009**, *324*, 1702−1704.
(80) Pagonis, D.; Price, D. J.; Algrim, L. B.; Day, D. A.; Handschy, A. V.; Stark, H.; Miller, S. L.; de Gouw, J.; Jimenez, J. L.; Ziemann, P. J. Time-resolved measurements of indoor chemical emissions, deposition, and reactions in a University Art Museum. *Environ. Sci. Technol.* **2019**, *53*, 4794−4802.
(81) Lelieveld, J.; Butler, T. M.; Crowley, J. N.; Dillon, T. J.; Fischer, H.; Ganzeveld, L.; Harder, H.; Lawrence, M. G.; Martinez, M.; Taraborrelli, D.; et al. Atmospheric oxidation capacity sustained by a tropical forest. *Nature* **2008**, *452*, 737−740.

https://doi.org/10.1021/acsearthspacechem.3c00004
ACS Earth Space Chem. 2023, 7, 1049−1059